



AIAA 2002-0982

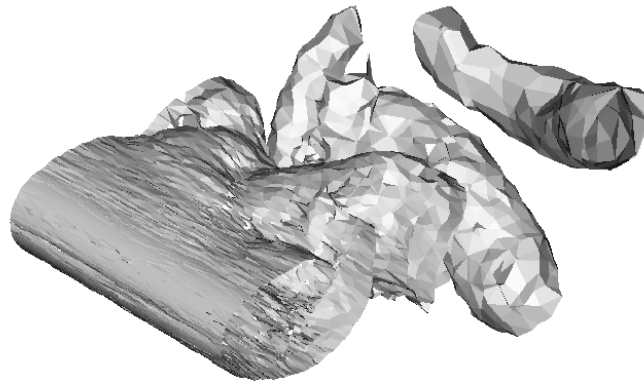
Large-Eddy Simulation of a Circular Cylinder on Unstructured Grids

Robert P. Hansen

United States Military Academy
West Point, NY

Lyle N. Long

The Pennsylvania State University
University Park, PA



**40th AIAA Aerospace Sciences
Meeting and Exhibit
14 – 17 January 2002 / Reno, NV**

LARGE-EDDY SIMULATION OF A CIRCULAR CYLINDER ON UNSTRUCTURED GRIDS

R. P. Hansen*

Department of Civil and Mechanical Engineering
United States Military Academy
West Point, New York 10996
Robert.Hansen@usma.edu

L. N. Long†

Department of Aerospace Engineering
The Pennsylvania State University
University Park, PA 16802
lnl@psu.edu

ABSTRACT

A computational study of unsteady, separated, low-Reynolds number fluid flow is made using a second-order accurate, cell-centered finite-volume method on unstructured grids. The three-dimensional simulations include large-eddy simulation turbulence modeling using a fixed-coefficient Smagorinsky subgrid-scale model. The flow about a three-dimensional circular cylinder at Reynolds number 3900 and Mach number 0.2 was studied using a standard Navier-Stokes formulation with and without the subgrid-scale modeling. A third case was also tested using a modified form of the Navier-Stokes equations with subgrid-scale modeling. Comparisons are made with experiment and selected three-dimensional numerical calculations performed on structured grids. The frequency of the unsteady vortex shedding was in good agreement with experiment, however, the numerical dissipation inherent in the upwind flux calculations affected the details of the time-averaged flowfield. The results showed an increased base pressure, shortened recirculation zones in the cylinder wake, and excessive drag compared to experiment for all cases.

Introduction

While problems involving flow over complex geometries have already been attempted using unstructured grid methods^{1,2,3}, the ability of unstructured methods to accurately simulate flow involving large-scale unsteadiness and turbulence has not been clearly demonstrated. The allure of accurately solving complex problems using the very efficient cell or element distribution offered by unstructured grids motivates continued research in this area.

The effectiveness of unstructured grid solutions for flow over standard geometries such as cubes and cylinders has not been systematically documented for both the large-scale mean properties and turbulent properties. The unsteady flow over a square cylinder⁴ and cube⁵ using unstructured grids has been studied as well as two-dimensional solutions for circular cylinders⁶ using unstructured methods. Numerous studies have provided critical insights into the advantages and disadvantages of various algorithms applied to three-dimensional cylinders using structured grids^{7,8,9,10}. The study of the three-dimensional circular cylinder using unstructured grid methods, however, is either scarce or non-existent. This paper presents results for a simulation of flow over a three-dimensional cylinder using an unstructured, cell-centered, finite-volume method.

The physics of flow about a circular cylinder is far more complex than its relatively simple shape might suggest. Despite being one of the most experimentally tested geometries in fluid mechanics, three-dimensional numerical studies of the circular cylinder have only been attempted in the last decade. Parallel computation, as well as more powerful vector computations, has made greater grid resolution possible, which in turn has made the use of LES feasible for problems requiring a large number of grid points. Direct Numerical Simulation of flow over a circular cylinder at a Reynolds number of 300 has even been accomplished¹¹. Much higher Reynolds numbers have been achieved using Detached - Eddy Simulation. Travin *et al.*¹² have computed results for the three-dimensional cylinder up to Reynolds number 3×10^6 .

Several experiments provide a very complete data set for flow over a circular cylinder at Reynolds number 3900. Norberg¹³ studied the effect of freestream turbulence on the measured flow, and provides surface pressure data as well as frequency of shedding for a range of Reynolds numbers. Krothapalli *et al.*¹⁴ and Lourenco and Shih¹⁵ measured time-averaged velocities and Reynolds stresses in the cylinder near-wake at Reynolds number 3900. Ong and Wallace¹⁶ provide experimental data at the same Reynolds number at positions further downstream of the cylinder, beyond the recirculation zone. These more recent, lower Reynolds number experiments have provided computational

* Assistant Professor, LTC, United States Army

† Professor, Associate Fellow, AIAA.

Copyright © 2002 by Hansen and Long. Published by the American Institute of Aeronautics and Astronautics, Inc. with permission

researchers with a test case that is easily within the capability of current computing power. At the Reynolds number of 3900 the attached boundary layer on the cylinder surface is laminar, the separated shear layers are in the early stages of transition, and the wake is fully turbulent.¹⁷ At this Reynolds number, the boundary layer is thick enough to be easily resolved by the computational grid. The experimental off-body data (pressure, velocities, Reynolds stresses) are also close enough to the cylinder so that an excessive number of computational cells in the cylinder wake can be avoided. Despite the fact that some part of the flowfield around a cylinder at Reynolds number 3900 is in transition, a condition that is obviously more difficult to compute, the overall advantages of using this Reynolds number are judged to outweigh any difficulties caused by the weakly transitional shear layers.

The computational results of Breuer⁷, Beaudan⁸, and Mittal¹⁸ for Reynolds number 3900 have added great insight into the advantages and disadvantages of various numerical schemes available on structured grids. Breuer⁷ used the Smagorinsky LES model with five different flux calculation schemes on a structured grid. He showed that the type of numerical scheme had a large impact on features of the time-averaged flowfield and parameters such as drag. Central difference approximation schemes produced more accurate results, while the schemes employing upwinding tended to shorten the recirculation bubble and predict excessive drag compared to experimental results.

Beaudan⁷ used a finite difference approach with fifth- and seventh-order upwind biased schemes to discretize the convective terms. His simulations for three cases -- no turbulence model, Smagorinsky LES model, and dynamic LES model -- all over-predict the length of the recirculation bubble, with the dynamic model falling within only two percent of the experimental value. Other characteristics of the recirculation bubble, such as the location and value of the maximum streamwise velocity along the wake centerline, were less accurate. Beaudan also evaluated the one-dimensional turbulence spectra at several downstream locations for both the fifth- and seventh-order accurate simulations.

While the main effort of this research is to evaluate a very difficult test case using unstructured grids, improvements in the solution accuracy were attempted by using a novel splitting method. Several researchers have used the technique of expressing the Navier-Stokes equations in terms of steady and unsteady components. Huia *et al.*¹⁹ used a decomposition of instantaneous variables similar to that done in the present research for investigating the evolution of a vortex in a three-dimensional boundary layer. Huia *et al.* decomposed each variable into a time-independent base flow and a time-dependent disturbance. By substituting this

decomposition into the Navier-Stokes equations and subtracting out the base flow, they formed what they called the disturbance equations

The splitting approach used here, called the nonlinear disturbance equations (NLDE), was first proposed by Morris *et al.*^{20,21,22} to compute solutions to high-speed circular and rectangular jet noise problems. The NLDE have since been successfully applied to a variety of viscous and inviscid problems.^{23,24,25,26,27} Hansen *et al.*²⁸ found the frequency of unsteady shedding over a two-dimensional cylinder to be more accurate using the NLDE formulation compared to a standard Navier-Stokes solution.

Governing Equations and Numerical Implementation

Governing Equations

The spatially filtered, time-dependent, Navier-Stokes equations are used. In integral form they are:

$$\frac{\partial}{\partial t} \iiint_V \tilde{Q} dV + \iint_S \tilde{F} \cdot \hat{n} dS = 0 \quad (1)$$

The conserved vector variable is given by:

$$\tilde{Q} = \begin{Bmatrix} \bar{\rho} \\ \bar{\rho}\tilde{u} \\ \bar{\rho}\tilde{v} \\ \bar{\rho}\tilde{w} \\ \bar{\rho}\tilde{E} \end{Bmatrix} \quad (2)$$

where the overbar indicates a spatially filtered quantity and the tilde ($\tilde{}$) denotes Favre (density weighting) averaging. The fluid density is given by ρ , the Cartesian velocity components are u , v , and w , and E is the energy per unit mass. The flux vector consists of:

$$\bar{F} = F_x \hat{i} + F_y \hat{j} + F_z \hat{k} \quad (3)$$

where

$$\tilde{F}_x = \begin{Bmatrix} \bar{\rho}\tilde{u} \\ \bar{\rho}\tilde{u}^2 + \bar{p} - \tilde{\tau}_{xx} + \tau''_{xx} \\ \bar{\rho}\tilde{u}\tilde{v} - \tilde{\tau}_{xy} + \tau''_{xy} \\ \bar{\rho}\tilde{u}\tilde{w} - \tilde{\tau}_{xz} + \tau''_{xz} \\ (\bar{\rho}\tilde{E} + \bar{p})\tilde{u} - \tilde{\tau}_{xx}\tilde{u} - \tilde{\tau}_{xy}\tilde{v} - \tilde{\tau}_{xz}\tilde{w} + \tilde{q}_x + \Theta''_x \end{Bmatrix}$$

$$\tilde{F}_y = \left\{ \begin{array}{l} \bar{\rho}\tilde{v} \\ \bar{\rho}\tilde{u}\tilde{v} - \tilde{\tau}_{xy} + \tau''_{xy} \\ \bar{\rho}\tilde{v}^2 + p - \tilde{\tau}_{yy} + \tau''_{yy} \\ \bar{\rho}\tilde{v}\tilde{w} - \tilde{\tau}_{yz} + \tau''_{yz} \\ (\bar{\rho}\tilde{E} + \tilde{p})\tilde{v} - \tilde{\tau}_{yx}\tilde{u} - \tilde{\tau}_{yy}\tilde{v} - \tilde{\tau}_{yz}\tilde{w} + \tilde{q}_y + \Theta''_y \end{array} \right\}$$

$$\tilde{F}_z = \left\{ \begin{array}{l} \bar{\rho}\tilde{w} \\ \bar{\rho}\tilde{u}\tilde{w} - \tilde{\tau}_{zx} + \tau''_{zx} \\ \bar{\rho}\tilde{v}\tilde{w} - \tilde{\tau}_{zy} + \tau''_{zy} \\ \bar{\rho}\tilde{w}^2 + p - \tilde{\tau}_{zz} + \tau''_{zz} \\ (\bar{\rho}\tilde{E} + \tilde{p})\tilde{w} - \tilde{\tau}_{zx}\tilde{u} - \tilde{\tau}_{zy}\tilde{v} - \tilde{\tau}_{zz}\tilde{w} + \tilde{q}_z + \Theta''_z \end{array} \right\}$$

$$\Theta''_i = \tau''_{ix} u + \tau''_{iy} v + \tau''_{iz} w - q''_i$$

The subgrid-scale (SGS) stresses and heat fluxes appear as τ''_{ij} and q''_i , respectively, in the above. Using the Smagorinsky model, the SGS stresses are defined by:

$$\tau''_{ij} = -2\mu_t \tilde{S}_{ij} \quad \mu_t = (C_s \Delta)^2 \bar{\rho} \sqrt{2\tilde{S}_{ij}\tilde{S}_{ij}} \quad (4)$$

where C_s is the Smagorinsky constant and is assigned a value of 0.1 in this study. The resolved deformation rate tensor is defined by:

$$\tilde{S}_{ij} = \frac{1}{2} \left(\frac{\partial \tilde{u}_i}{\partial x_j} + \frac{\partial \tilde{u}_j}{\partial x_i} \right) \quad (5)$$

The model for the SGS heat fluxes is:

$$q''_i = \frac{\gamma \mathcal{R}}{\gamma - 1} \frac{\mu_t}{Pr_t} \frac{\partial \tilde{T}}{\partial x_i} \quad (6)$$

where Pr_t is the turbulent Prandtl number and is commonly chosen in the range of 0.3 to 0.5.

The major shortcoming of the fixed-coefficient Smagorinsky model is its behavior close to the wall. In the boundary layer, the ‘‘large’’ scale eddies approach the size of the small scales. The typical grid is too coarse in the boundary layer, causing the Smagorinsky model to create excessive dissipation. One method of correcting this is to damp out the turbulent viscosity contribution near the wall. Use of a van Driest damping function with LES provides the required reduction in eddy viscosity near the wall. The Smagorinsky coefficient in equation 4 is replaced by C_s^* defined as:

$$C_s^* = C_s \sqrt{1 - e^{(-y^+/A^+)^3}} \quad (7)$$

where A^+ is a constant equal to 25.0, and y^+ is the distance, in viscous wall units, from the wall to the field point where eddy viscosity is to be evaluated. The viscous wall unit is defined by:

$$y^+ = \frac{d}{\nu} \sqrt{\frac{\tau_w}{\rho_w}} \quad (8)$$

where d is the distance from a cell center to the nearest face that is on a viscous surface, τ_w is the shear stress at the wall, ρ_w is the fluid density at the wall, and ν is the coefficient of dynamic viscosity. Calculation of y^+ on a partitioned, unstructured grid requires particular care and is discussed in the section on numerical implementation.

Use of the nonlinear disturbance equations (NLDE) requires the resolved-scale variables to be decomposed into a mean quantity that is independent of time and a time-dependent perturbation. For example:

$$\begin{aligned} \bar{\rho}(x,t) &= \rho_o(x) + \rho'(x,t) \\ \tilde{u}(x,t) &= u_o(x) + u'(x,t) \end{aligned} \quad (9)$$

The decomposition of each variable is substituted into the filtered equations, and the terms containing purely mean flow quantities are placed on the right-hand side, so that equation 1 may now be written as:

$$\frac{\partial}{\partial t} \iiint_V Q' dV + \iint_S F' \cdot \hat{n} dS + \iint_S F'' \cdot \hat{n} dS = R_o \quad (10)$$

where

$$R_o = -\frac{\partial}{\partial t} \iiint_V Q_o dV - \iint_S F_o \cdot \hat{n} dS$$

$$Q' = \left\{ \begin{array}{l} \rho' \\ \rho_o u' + \rho' u_o + \rho' u' \\ \rho_o v' + \rho' v_o + \rho' v' \\ \rho_o w' + \rho' w_o + \rho' w' \\ e' \end{array} \right\}$$

$$F_x' = \left\{ \begin{array}{l} \rho_o u' + \rho' u_o + \rho' u' \\ \rho' u_o^2 + 2\rho_o u_o u' + \rho' u_o^2 + \rho' u'^2 + 2\rho' u' u_o - \tau_{xx}' \\ \rho_o u_o v' + \rho_o v_o u' + \rho' u_o v_o + \rho_o u' v' + \rho' v' u_o + \rho' u' v_o + \rho' u' v' - \tau_{xy}' \\ \rho_o u_o w' + \rho_o w_o u' + \rho' u_o w_o + \rho_o u' w' + \rho' w' u_o + \rho' u' w_o + \rho' u' w' - \tau_{xz}' \\ e'(u_o + p_o) + u_o(e' + p') + u'(e' + p') - \Theta_x' \end{array} \right\}$$

$$F_x'' = \begin{Bmatrix} 0 \\ \tau_{xx}'' \\ \tau_{xy}'' \\ \tau_{xz}'' \\ \Theta_x'' \end{Bmatrix}$$

$$\Theta_i' = \tau_{ix}' (u_o + u') + \tau_{oix} u' + \tau_{iy}' (v_o + v') + \tau_{oiy} v' + \tau_{iz}' (w_o + w') + \tau_{oiz} w' - q_i'$$

$$\Theta_i'' = \tau_{ix}'' (u_o + u') + \tau_{iy}'' (v_o + v') + \tau_{iz}'' (w_o + w') - q_i''$$

The remaining components of F' and F'' are similarly expanded. The variable Q' in equation 10 is a new vector of conserved variables consisting of only interactions between the perturbations themselves or the perturbations and the mean flow. F'' contains all of the SGS stresses and heat fluxes, and Q_o and F_o are the same as defined by equations 2 and 3 except all terms are now resolved mean quantities. Depending on how the mean flow is obtained, the value of R_o may or may not be zero²⁸. When R_o is a constant it is calculated only once at the beginning of a computation. A steady, uniform flow is chosen as the mean flow in this study, reducing R_o to zero.

Numerical Implementation

The governing equations are discretized using a second-order accurate, cell-centered finite-volume method with upwinding for stability. The code used in this research is FLOUS (FLOW UnStructured), originally written by Long²⁹ in Connection Machine FORTRAN (CMF). Weinberg and Long³⁰ later modified this code to use adaptive meshing. The present research included updating of the FLOUS code to FORTRAN90 and the addition of Message Passing Interface (MPI) library subroutine calls to allow parallel operation. Large-eddy simulation, in the form of a constant coefficient Smagorinsky model, was also added for turbulence modeling. The upwinding technique employs Roe's flux difference splitting³¹. A standard 4th order Runge-Kutta integration is used to explicitly advance the solution in time. Unstructured grids composed of tetrahedral cells were generated using the Gridtool/VGRIDns 3.3 software^{32,33}. The grid was decomposed into subdomains or zones using the METIS 4.0 partitioning software³⁴. Several utilities were also written for FLOUS to handle a variety of pre- and post-processing tasks.

Parallel operation of the code using MPI requires the exchange of all conserved variables between the cells

on either side of a face that defines a zonal boundary. This exchange occurs several times per time step. Additional message passing requirements are incurred when calculating the eddy viscosity damping given by equation 7. Equation 8 implies an association between each cell center and the nearest solid, viscous face. Each cell identifies the location of and distance from its nearest wall face once as the code initializes. In a partitioned, unstructured grid the cell and its nearest solid surface may not be part of the same zone. This requires information, specifically the shear stress and the density, at the wall be sent from the face center to the cell where eddy viscosity is to be evaluated. This additional message passing takes place each time step.

Simulations and Results

Simulations

A circular cylinder in a crossflow at Reynolds number 3900 has been simulated at Mach = 0.2. The cylinder is four diameters in span. A symmetry boundary condition is placed at the end walls, creating the effect of an inviscid wall. Figure 1 shows the surface grid of the cylinder. Approximately 28 cells define the cylinder surface in the spanwise(y) direction, or seven cells per diameter. The farfield boundaries are placed 10 diameters from the cylinder surface except for the downstream exit plane, which is 20 diameters from the cylinder. The complete grid consists of 308,208 tetrahedral cells. All time-averages are computed using ten cycles of shedding. Spanwise averaging is also performed using 13 points across the span.

All computations were done on the NASA Ames Research Center 512-processor Origin 2000 system (LOMAX cluster) using 64 processors. Each cycle of shedding required approximately 2.8 hours of wall time, or about 0.25 seconds per iteration per cell.

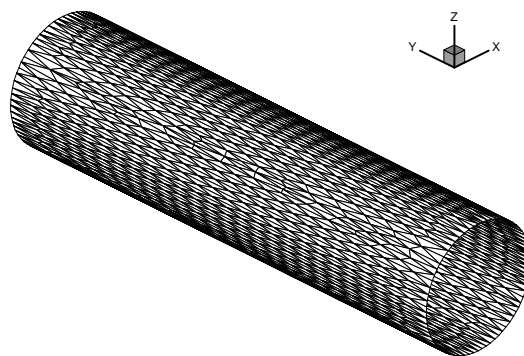


Figure 1. Surface Mesh of the Circular Cylinder

Three cases are compared – the baseline FLOUS code without LES turbulence modeling, the baseline

Table 1. Key Parameters for the Three-Dimensional Cylinder Computation

| | C_D | C_{pb} | St | L_r/D |
|-------------------------------|-----------------|------------------|-----------|----------------|
| Baseline FLOUS | 1.308 | -1.361 | 0.237 | 0.732 |
| FLOUS w/ LES | 1.312 | -1.339 | 0.207 | 0.635 |
| NLDE w/ LES | 1.388 | -1.490 | 0.205 | 0.561 |
| Breuer ⁷ , Case B2 | 1.319 | -1.432 | OK | 0.630 |
| Breuer ⁷ , Case D3 | 1.016 | -0.941 | OK | 1.372 |
| Experiment ¹³ | 0.98 ± 0.05 | -0.90 ± 0.05 | 0.20-0.22 | 1.33 ± 0.2 |

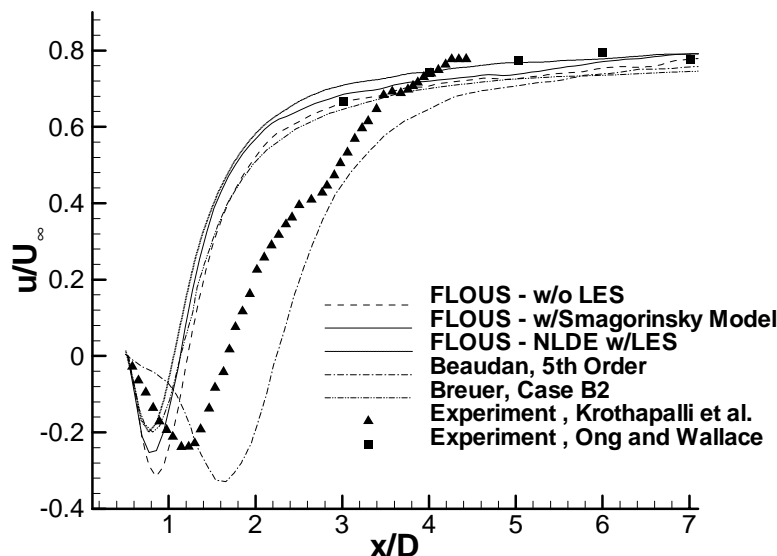


Figure 2. Time-Averaged Velocity Along the Wake Centerline

FLOUS code with LES turbulence modeling, and the NLDE formulation with LES modeling. A summary of key time-averaged parameters is given in Table 1. The computed coefficient of drag, C_D , is substantially higher in all cases than the experimental value. The base pressure coefficient, C_{pb} , is defined as the coefficient of pressure at the point on the cylinder surface furthest downstream. The magnitude of C_{pb} is also larger than the experimental value for all cases. The Strouhal number is slightly above the experimental value for the baseline code, but falls within the experimental range for the cases with LES. The case B2 from Breuer⁷ is used for comparison because that case used an upwind approximation for flux calculations. The Strouhal number for this case was not provided, but Breuer stated it was within the range of experiment. The length of the recirculation bubble, L_r , is non-dimensionalized by the cylinder diameter as L_r/D in the last column of Table 1. There is a direct correlation between the drag coefficient and the length of the recirculation bubble – the shorter the recirculation zone the higher the drag coefficient.

Figure 2 shows the time-averaged streamwise velocity along the wake centerline for all cases. Also

shown are experimental results and selected results from Beaudan⁸ and Breuer⁷. The mean flow is in the positive x -direction in all figures and the distance along the wake is non-dimensionalized by the cylinder diameter. In all the present cases, the recirculating zone is significantly shorter than it should be. The cases using LES are very similar to the Breuer case B2 that uses a Smagorinsky subgrid-scale model and an upwind scheme for the flux calculations.

The addition of LES to the baseline code has the desirable effect of correcting the minimum velocity in the recirculating zone to a value consistent with experiment. The length of the recirculating zone is, however, slightly shortened when LES is added. Use of the NLDE formulation shortens the recirculating zone even further and reduces the minimum velocity in the bubble to a value below the experimental value.

Figure 3 shows the time-averaged, span-averaged streamlines for the NLDE model. This case has the shortest time-averaged recirculation zone, but is otherwise qualitatively the same as the non-NLDE cases. Figure 4 shows the time-averaged streamlines for a three-dimensional numerical computation from Breuer⁷

(case D3) which used a central difference approximation scheme with a dynamic subgrid-scale LES turbulence model. All parameters of this simulation are very close to the experimental ranges, and the time-averaged streamlines are also accepted to be an accurate representation of the experimental data. Comparison of Figure 3 and Figure 4 show the time-averaged recirculation zone of the present study to be less than half the length of the Breuer case D3, consistent with the data in Table 1. Additionally, the two smaller, counter-rotating vortices seen in Figure 3 are absent from Figure 4.

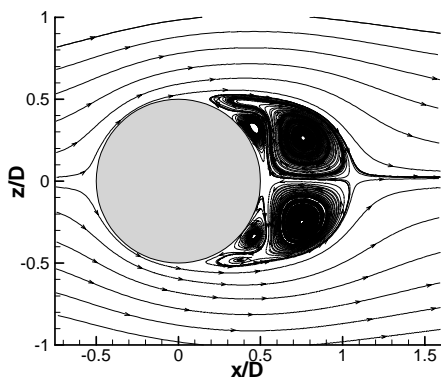


Figure 3. Time-Averaged Streamlines for the NLDE Case

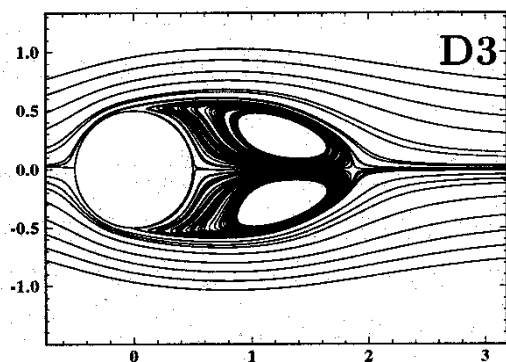


Figure 4. Time-Averaged Streamlines from Breuer (reference 7) Case D3

Figure 5 reveals the strong three-dimensional flow that results from performing the cylinder computation in three dimensions. Shown is an iso-surface of absolute vorticity. Such three-dimensionality was absent when similar computations were performed during the present research using grids only two diameters in span.

The reason for the poor performance of all cases in the areas of drag, base pressure coefficient, and length of the recirculating zone appears to be related to the use of upwinding. Breuer⁷ was able to obtain significantly better results than the B2 case used here for comparison

by using central difference approximations. The inherent numerical dissipation in Roe's upwinding scheme, used in the present research, appears to be excessive, causing the wake to be dominated by the largest scales. This results in a wake pressure that is too low and a drag that is too high.

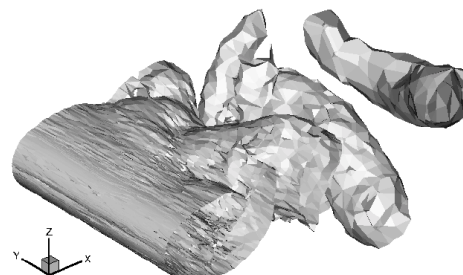


Figure 5. Iso-Surface of Absolute Vorticity

Figure 6 shows the instantaneous vorticity structure on the center-plane perpendicular to the cylinder axis obtained from the baseline FLOUS code. The structure of the vorticity in the wake is very similar to that obtained from a purely two-dimensional simulation. The wake is dominated by large coherent structures. Much smaller scale motion should be superimposed on the periodic vortex shedding. The oversized large-scale motion also appears responsible for inducing the counter-rotating smaller vortex adjacent to the cylinder surface.

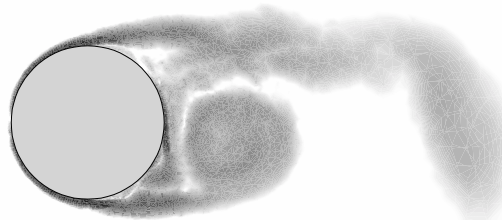


Figure 6. Instantaneous Vorticity Magnitude (darker shading indicates higher vorticity magnitude)

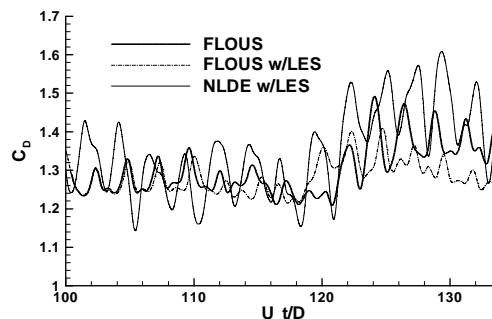


Figure 7. Drag Coefficient Time History

The drag and lift coefficient time-histories for approximately six and one-half shedding cycles are shown in Figure 7 and Figure 8. While the time-

averaged value of drag is too high, the time variations are consistent with experiment and other numerical studies. The peak-to-peak fluctuations are also smaller for the three-dimensional simulations compared to the two-dimensional case, although the three-dimensional NLDE case allows larger drag fluctuations than the other two.

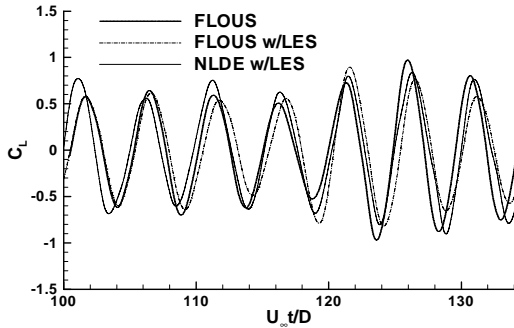


Figure 8. Lift Coefficient Time History

A comparison of the Reynolds stresses with experimental data was also made. All Reynolds stress components are normalized by U_∞^2 . Figure 9 compares the streamwise normal Reynolds stress ($\overline{u'u'}$) of the different cases. The near wake appears very similar for all cases. Only further downstream are some differences observable.

Figure 10 shows the streamwise Reynolds normal stress component ($\overline{u'u'}$) at the location $x/D = 1.54$ behind the cylinder. The streamwise components computed by the baseline code and the baseline code with LES under-predict the peak Reynolds stresses by as much as 12%. The NLDE version predicts the peaks to within one percent, but the locations of the peaks are slightly displaced from the experimental locations. It should be noted that there is a degree of uncertainty of the exact peak of the experimental data based on the fact that a number of curves could fit the data providing different peaks. Percentage differences used in this discussion are relative to the largest values plotted.

Figure 11 shows the $\overline{u'w'}$ Reynolds shear stress component for the NLDE case in the xz plane. Figure 12 shows the shear stress value at $x/D = 1.54$ for all cases. All the cases over-predict the shear Reynolds stress by as much as 36%. The baseline FLOUS code using LES appears to be slightly more accurate than the other cases, but is still 27% over the experimental value. The $\overline{w'w'}$ lateral normal Reynolds stress component is shown in Figures 13 and 14. All calculations significantly over-predict the $\overline{w'w'}$ component by at least 100%. The calculations of Mittal¹⁸ also significantly over-predict the magnitude of this component. Breuer⁷ successfully captures this

component when using a dynamic LES model with central difference approximations.

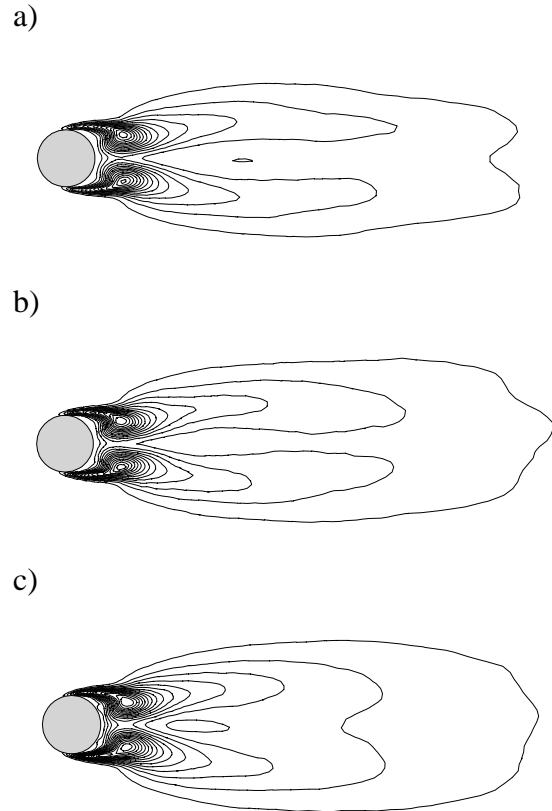


Figure 9. Streamwise Reynolds Normal Stress in the xz Plane: (a) FLOUS, (b) FLOUS w/LES, (c) NLDE w/LES; (15 contours from 0.025 to 0.400)

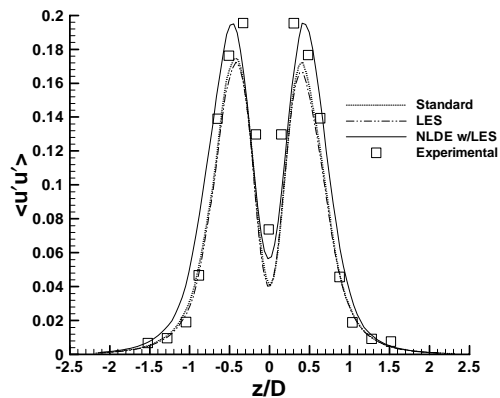


Figure 10. Streamwise Reynolds Normal Stress at $x/D = 1.54$ (experimental data from reference 15)

The spanwise ($\overline{v'v'}$) Reynolds normal stress is shown in Figure 15 in the plane perpendicular to the cylinder axis. Figure 16 shows the spanwise stress at

$x/D = 1.54$ for the NLDE case against two other numerical simulations. The results of Beaudan⁸ are used as the benchmark because experimental data is not available for this component. The peak stress value from Beaudan is 35% higher than the NLDE case or Mittal's¹⁸ calculation. Figure 16 indicates a reduced level of three-dimensionality in the near-wake for the present study. The reduced spanwise stresses contribute to the higher values of the in-plane $\overline{u'w'}$ and $\overline{w'w'}$ components. This precise condition has been shown by Mittal and Balachandar³⁵ to lead to a higher value of base pressure coefficient and higher drag.

Both Beaudan⁸ and Mittal¹⁸ used grids with approximately 15 cells per diameter along the span of the cylinder, or roughly twice the spanwise density used in this study. Despite the differences in grid density between the present study and Mittal, who used a second-order finite difference method, the peak value for spanwise Reynolds stress is the same. This indicates that the seventh-order scheme used by Beaudan accounts for the better accuracy of his results, and not the grid density.

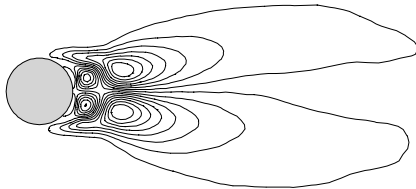


Figure 11. Reynolds Shear Stress in the xz Plane – NLDE (15 contours from -0.165 to 0.192)

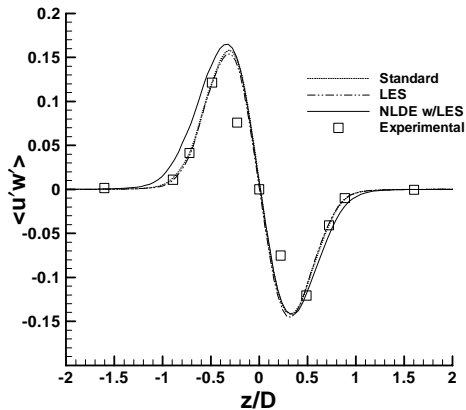


Figure 12. Reynolds Shear Stress at $x/D = 1.54$ (experimental data from reference 15)

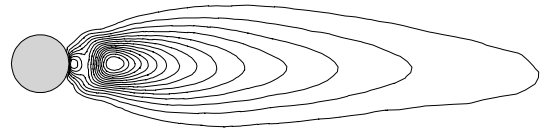


Figure 13. Lateral Reynolds Normal Stress in the xz Plane – NLDE (15 contours from 0.090 to 0.810)

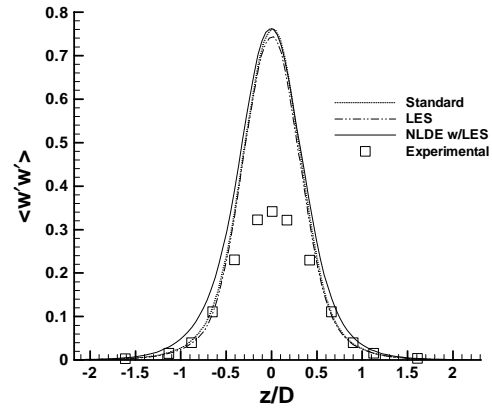


Figure 14. Lateral Reynolds Stress at $x/D = 1.54$ (experimental data from reference 15)

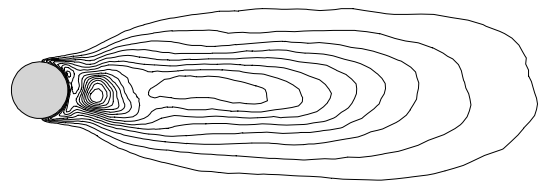


Figure 15. Spanwise Reynolds Normal Stress in the xz Plane – NLDE (15 contours from 0.01 to 0.10)

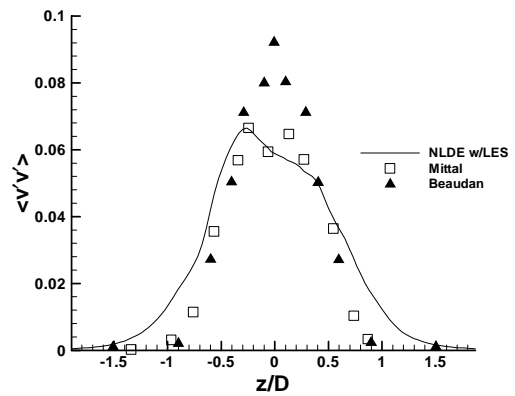


Figure 16. Spanwise Reynolds Normal Stress at $x/D = 1.54$ (Mittal – Run II from reference 18, Beaudan – Fifth-order from reference 8)

CONCLUSIONS

The accuracy of the three-dimensional cylinder drag, base pressure, shedding frequency, and length of the recirculation zone were all degraded by application of the NLDE method. The only benefit from using the NLDE form was a modest improvement in the peak normal Reynolds stress in the streamwise direction.

The application of Large Eddy Simulation using a fixed-coefficient Smagorinsky model had a noticeable effect on key parameters of the three-dimensional cylinder tests. Relative to the baseline FLOUS code, the Strouhal number was more accurate and the minimum velocity in the recirculating zone was noticeably improved when LES was used. The overall poor quality for all three-dimensional cylinder cases is attributed primarily to the upwinding used in the finite-volume formulation. The use of upwinding introduces undesirable levels of artificial dissipation. Grid refinements studies should be conducted, however, to separate the effects of grid resolution and dissipation caused by upwinding on the accuracy of these results.

The artificial dissipation inherent in upwinding is necessary, to an extent, for numerical stability. Other researchers^{7,18} have shown that central difference approximation schemes are superior on structured grids. The central difference schemes, however, require the explicit addition of artificial dissipation for numerical stability. Explicit artificial dissipation is not a current capability on three-dimensional unstructured grids, limiting unstructured methods to the use of upwinding. While the structured, higher-order, upwinded method used by Beaudan⁸ performed better than the method used in the present research, dependable higher order methods for unstructured finite-volume grids have not been developed. The ultimate effect of excessive dissipation experienced in the three-dimensional cylinder cases is the domination of large-scale vortices in the cylinder near-wake, leading to a pressure that is too low and a drag prediction that is excessive.

References

¹Mineck, R., "Application of an Unstructured Grid Navier-Stokes Solver to a Generic Helicopter Body - Comparison of Unstructured Grid Results with Structured Grid Results and Experimental Results", NASA TM 1999-209510.

²Frink, N. and Pirzadeh, S. "Tetrahedral Finite-Volume Solutions to the Navier-Stokes Equations on Complex Configurations". NASA / TM-1998-208961, December 1998.

³Grismer, M., Strang, W., Tomaro, R., and Witzeman, F. "Cobalt: A Parallel, Implicit, Unstructured Euler/Navier-Stokes Solver". *Advances in Engineering Software*, Vol. 29, No. 3-6, 1998.

⁴Camarri, S. and Salvetti, M.V. "Towards the Large-Eddy Simulation of Complex Engineering Flows with Unstructured Grids", INRIA Report 3844, December 1999.

⁵Shah, K. and Ferziger, J. "A Fluid Mechanics View of Wind Engineering: Large Eddy Simulation of Flow Past a Cubic Obstacle". *Journal of Wind Engineering and Industrial Aerodynamics*, Vol. 67 and 68, pp. 211-224, 1997.

⁶Selvam, R.P. "Finite Element Modeling of Flow Around a Circular Cylinder using LES", *Journal of Wind Engineering and Industrial Aerodynamics*, Vol. 67 and 68, 1997.

⁷Breuer, M. "Large Eddy Simulation of the Sub-Critical Flow Past a Circular Cylinder: Numerical and Modeling Aspects". *International Journal for Numerical Methods in Fluids*, Vol. 28, No. 9, pp. 1281-1302, December 1998.

⁸Beaudan, P., and Moin, P., "Numerical Experiments on the Flow Past a Cylinder at Sub-Critical Reynolds Number", report No. TF-62, Department of Mechanical Engineering, Stanford University, 1994.

⁹Mittal, S. "Computation of Three-Dimensional Flows Past a Circular Cylinder of Low Aspect Ratio", *Physics of Fluids* 13, 2001.

¹⁰Kravchenko, A., and Moin, P., "Numerical Studies of Flow Over a Circular Cylinder at $Re_D=3900$ ", *Physics of Fluids* 12, 2000.

¹¹Mittal, R. and Balachandar, S. "Generation and Evolution of Vortical Structures in Bluff Body Wakes". 34th Aerospace and Sciences Meeting and Exhibit. AIAA Paper 96-0210, 1999.

¹²Travin, A., Shur, M., Strelets, M., and Spalart, P., "Detached-Eddy Simulations Past a Circular Cylinder", *Flow Turbulence and Combustion* 63: 293-313, 1999.

¹³Norberg, C., "Effects of Reynolds Number and Low-Intensity Free-Stream Turbulence on the Flow Around a Circular Cylinder". Publication 87/2, Department of Applied Thermosciences and Fluid Mechanics, Chalmers University of Technology, Gothenburg, Sweden, 1987.

- ¹⁴Krothapalli, A., Shih, C., and Lourenco, L. "The Near Wake of a Circular Cylinder at $0.3 < M_\infty < 0.6$: a PIV Study". 32nd Aerospace Sciences Meeting and Exhibit, AIAA Paper 94-0663, 1994.
- ¹⁵Lourenco, L., and Shih, C., "Characteristics of the Plane Turbulent Near Wake of a Circular Cylinder, A Particle Image Velocimetry Study". Private Communication, 1993 (data taken from reference 18)
- ¹⁶Ong, L. and Wallace, J. "The Velocity Field of the Turbulent Very Near Wake of a Circular Cylinder". *Experiments in Fluids*, Vol. 20, pp. 441-453, 1996.
- ¹⁷Zdravkovich, M., *Flow Around Circular Cylinders*, Oxford University Press, Oxford, 1997.
- ¹⁸Mittal, R. "Large-eddy Simulation of Flow Past a Circular Cylinder". Annual Research Briefs, Center for Turbulence Research, Stanford University, 1995.
- ¹⁹Huai, X., Joslin, R.D. and Piomelli, U. "Large Eddy Simulation of Boundary Layer Transition on Swept Wings", *ICASE/LaRC Workshop on Transition, Turbulence, and Combustion*, Hampton, VA, June 2 – July 7, 1993.
- ²⁰Morris, P.J., Long, L.N., Bangalore, A., Wang, Q., "A Parallel Three-Dimensional Computational Aeroacoustics Method Using Nonlinear Disturbance Equations", *J. of Computational Physics*, Vol. 133, 1997.
- ²¹Morris, P.J., Long, L.N., Lockard, D.P., Wang, Q., "Numerical Prediction of High Speed Jet Noise", AIAA Paper 97-1598, 1997.
- ²²Morris, P.J., Long, L.N., Scheidegger, T.E., Wang, Q., Pilon, A.R., "High Speed Jet Noise Simulations", AIAA Paper 98-2290, 1998.
- ²³Liu, J., Long, L.N., Modi, A., "Higher Order Accurate Solutions of Ship Airwake Flow Fields using Parallel Computers", AGARD Conference, Amsterdam, 1998.
- ²⁴Liu, J., Long, L.N., "Direct Aeroacoustic and Aerodynamic Simulation of Multi-Hole Engine Liners", AIAA Paper 98-2330, 1998.
- ²⁵Chyczewski, T, Morris, P.J., and Long, L.N., "Large-Eddy Simulation of Wall Bounded Shear Flow Using the NLDE", AIAA Paper 2000-2007, 2000.
- ²⁶Long, L.N., "A Non-Conservative Nonlinear Flowfield Splitting Method", AIAA Paper 2000-1998, 2000.
- ²⁷Sezer-Uzol, N. and Long, L.N., "High Accuracy Wake and Vortex Simulation Using a Hybrid CFD/DV Method", AIAA Paper 2000-2029, 2000.
- ²⁸Hansen, R.P., Long, L.N., and Morris, P.J., "Unsteady, Laminar Flow Simulations Using the Nonlinear Disturbance Equations", *6th AIAA/CEAS Aeroacoustics Conference*, AIAA Paper 2000-1981, Maui, June, 2000.
- ²⁹Long, L.N., "Parallel Algorithms for Gas Dynamics". In *Parallel Computational Fluid Dynamics '92*, Elsevier Science Publishers, Amsterdam, pp. 279-289, 1993.
- ³⁰Weinberg, Z. and Long, L.N., "A Massively Parallel Solution of the Three-Dimensional Navier-Stokes Equations on Unstructured Grids", AIAA Paper 94-0760, 1994.
- ³¹Roe, P. "Approximate Riemann Solvers, Parameter Vectors, and Difference Schemes". *Journal of Computational Physics*, Vol. 43, pp. 357-372, 1981.
- ³²Samareh, J. "Gridtool: A Surface Modeling and Grid Generation Tool". Proceeding of the Workshop on Surface Modeling, Grid Generation, and Related Issues in CFD Solutions, NASA CP-3291, May 1995.
- ³³Pirzadeh, S. "Viscous Unstructured Three-Dimensional Grids by the Advancing-Layers Method", AIAA Paper 94-0417, 1994.
- ³⁴Karypis, G. and Kumar, V. "METIS – A Software Package for Partitioning Unstructured Graphs, Partitioning Meshes, and Computing Fill-Reducing Ordering of Sparse Matrices, Version 4.0". University of Minnesota, Department of Computer Science/Army HPC Research Center, Minneapolis, MN 55455, September 1998.
- ³⁵Mittal, R. and Balachandar, S. "Effect of Three-Dimensionality on the Lift and Drag of Nominally Two-Dimensional Cylinders". *Physics of Fluids* 7 (8), August 1995, 1841-1865.